Supplementary Materials for

In situ fabricated quasi-solid polymer electrolyte incorporated by ionic liquid for flexible supercapacitor

Hai Lu[1], Peichun Wang[1], Yitian Ma[1*], Meng Liu[1], Linqing Chang[1], Rui Feng[1], Shuliang Luo[1], Zhiyun Zhang[1], Yi Wang[2], Yan Yuan[3*]

[1]School of Materials Science and Engineering, Xi'an University of Science and Technology, Xi'an 710054, China

[2]School of Materials Science and Engineering, Hunan University of Science and Tech nology, Xiangtan 411201, China

[3]School of Metallurgical Engineering, Xi'an University of Architecture and Technology, Xi'an 710055, China

[*] Corresponding author 1#: Tel.: +86 29 85587373
E-mail address: ytma@xust.edu.cn

[*] Corresponding author 2#: Tel.: +86 29 82202923
E-mail address: lingyi21@126.com

Supplementary Notes

The ionic conductivity of the QSPE was calculated according to Eq. (1)[1]:

$$\sigma = \frac{L}{R \times A} \tag{1}$$

Where L and A is the thickness and area of the QSPE, respectively, and R is the bulk resistance from EIS measurement of the symmetrical stainless steel cell.

The relationship between logσ and T^{-1} in Fig.2c was linearly fitted and then activation energy (E_a) of the QSPE was obtained according to Eq. (2) [2]:

$$\sigma(T) = A\exp\left(-\frac{E_a}{kT}\right) \tag{2}$$

Where A is pre-exponential factor, k is Boltzmann constant, and T is the absolute temperature.

The ion diffusion coefficient D, exchange current density i_0 and time constant τ was calculated by Eq. (3), Eq. (4) and Eq. (5), respectively, based on the EIS result of the capacitor [3-5]:

$$D = \frac{R^2T^2}{2A^2n^4F^4C^2{\sigma_0}^2} \tag{3}$$

Where R is the ideal gas constant, F is the Faraday constant, T represents the absolute temperature, A is the electrode area, n is the number of transferred electrons per molecule during the electrode reaction, C is the molar concentration of electrolyte, σ_0 is the Warburg impedance.

$$i_0 = \frac{RT}{nFAR_{ct}} \tag{4}$$

Where R_{ct} is the charge transfer resistance, obtained by the diameter of the semicircle in the high-frequency region of the EIS.

$$\tau = \frac{L^2}{D} \tag{5}$$

Where L is the ion diffusion distance approximating the electrolyte thickness between two electrodes, and D is the ion diffusion coefficient.

The specific capacitance C_s of the single electrode was calculated according to Eq. (6), based on charge/discharge test of the capacitor [6]:

$$C_s = \frac{I\ \Delta t}{m\Delta V} \times 4 \tag{6}$$

Where m is the total mass of two electrodes, I is the discharge current, Δt is the discharge time, and ΔV is discharge voltage interval after removing the IR drop.

The C_s value can also be obtained according to Eq. (7), based on the CV measurement of the capacitor [7]:

$$C = \frac{\int IdV}{2mv\Delta V} \tag{7}$$

Where the integral part represents the area inside the CV, m is the total mass of the two electrodes, v is the scan rate and ΔV is the operating voltage window.

The specific energy E (Wh kg^{-1}) and specific power P (W kg^{-1}) of the capacitor was calculated according to Eq. (8) and Eq. (9), respectively [8]:

$$E = \frac{1}{8 \times 3.6} C_s \Delta V^2 \tag{8}$$

$$P = \frac{E}{\Delta t} \times 3600 \tag{9}$$

Supplementary Figures

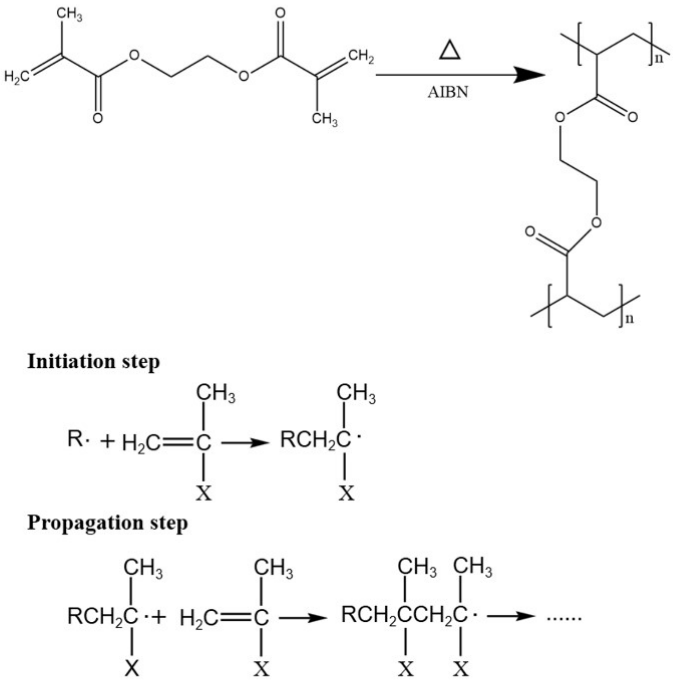

Fig.S1 Free radical polymerization mechanism of PEGDMA induced by AIBN under thermal condition

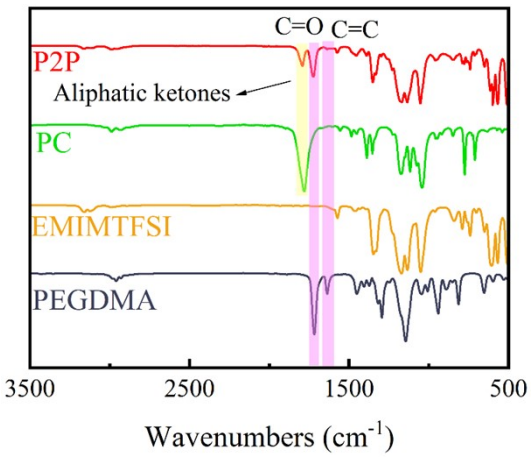

Fig.S2 FTIR spectra of P2P and its corresponding components

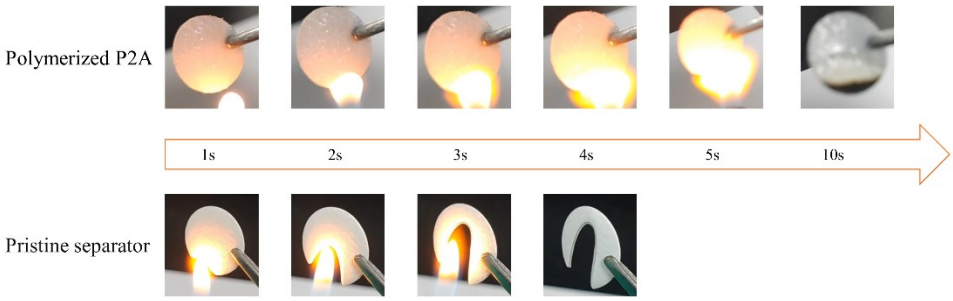

Fig.S3 Pictures of the ignition test on the P2A and cellulose separator

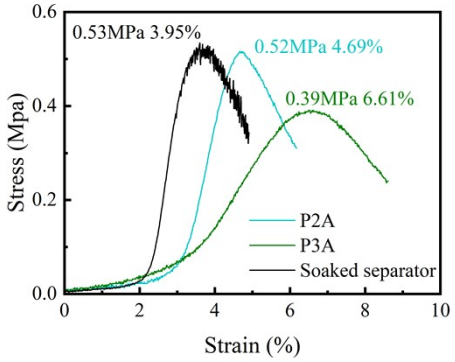

Fig.S4 Stress-strain curves of P2A, P3A and cellulose separator soaked in the IL

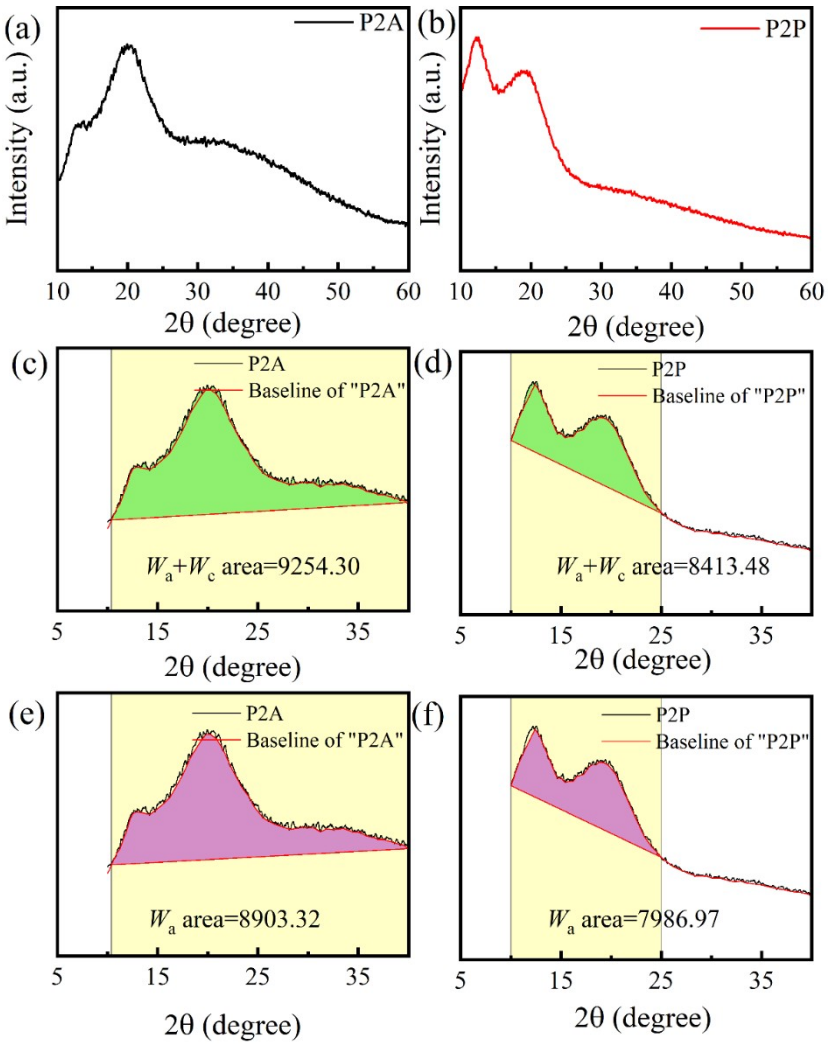

Fig.S5 XRD patterns of (a, c, e) P2A and (b, d, f) P2P, (c、d、e、f). W_c and W_a represent the area of the crystalline and amorphous region, respectively. The crystallinity fraction X_c was calculated as follows [9]:

$$X_c = \frac{W_c}{W_c + W_a} * 100\%$$

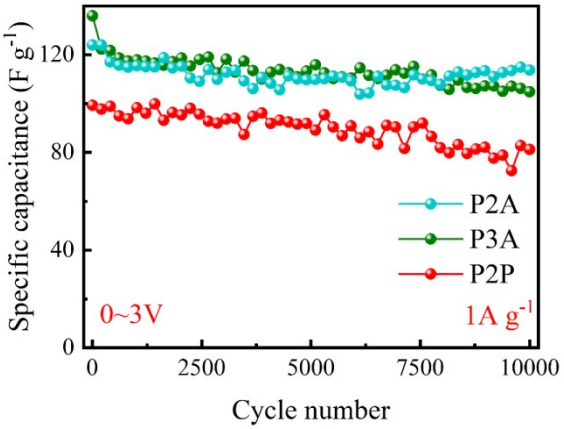

Fig.S6 Comparison of cycle performance of the SCs with three ILQSEs at 1A g^{-1}

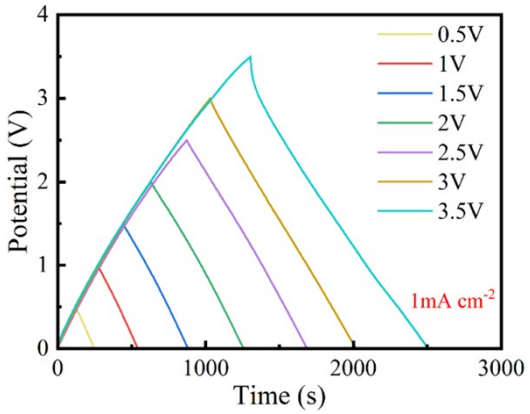

Fig.S7 GCD curves of the SC with P2A at different cut-off voltages

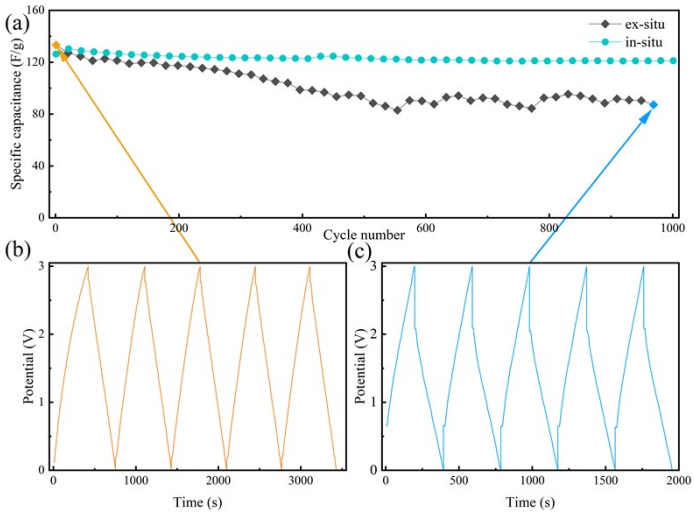

Fig.S8 (a) Cycle performances of the SCs with *in-situ* and *ex-situ* prepared P2A; Charge-discharge curves of the SCs with *ex-situ* prepared P2A at (b) initial cycles and (c) later cycles

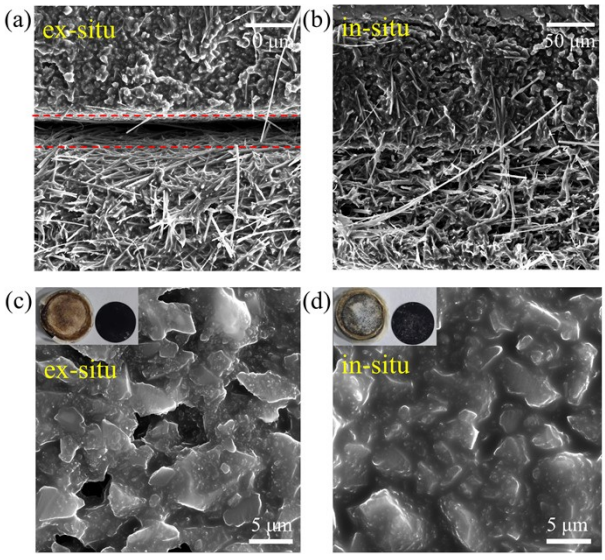

Fig.S9 Cross-section images of the cycled AC electrodes adhered by the (a) *ex-situ* prepared P2A

and (b) *in-situ* prepared P2A; Surface morphologies of the cycled AC electrodes after (c) *ex-situ* prepared P2A and (d) *in-situ* prepared P2A were peeled off from the electrode surface

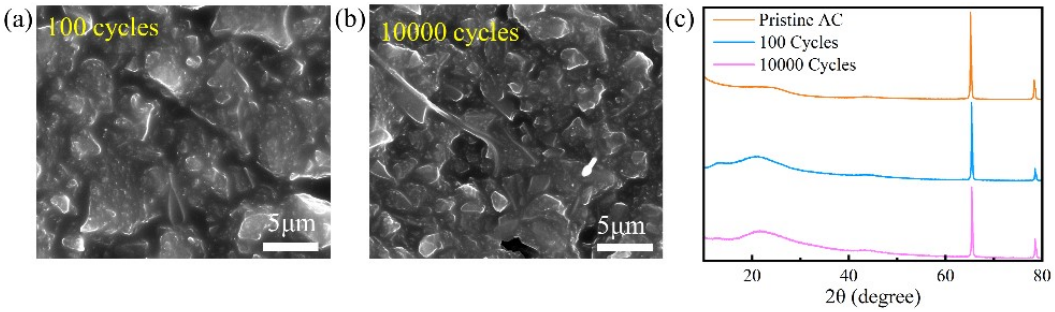

Fig.S10 SEM images of the AC electrode (a) after 100 cycles and (b) after 10000 cycles; (c) Comparison of XRD patterns of the AC electrode during cycling (the *in-situ* prepared P2A were peeled off from the cycled electrode)

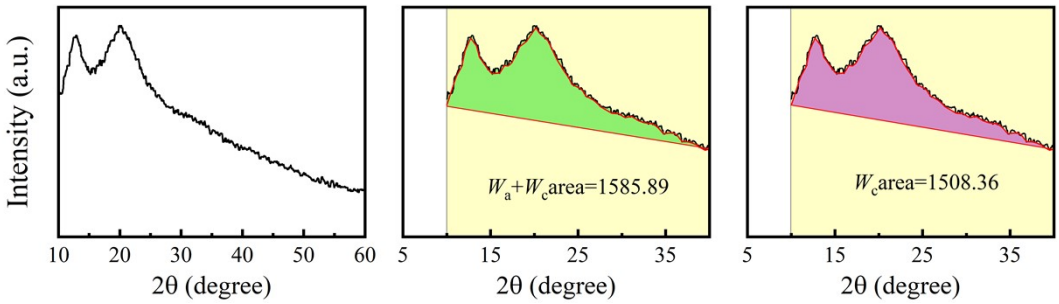

Fig.S11 XRD patterns of the *in-situ* prepared P2A peeled off from the cycled AC electrode

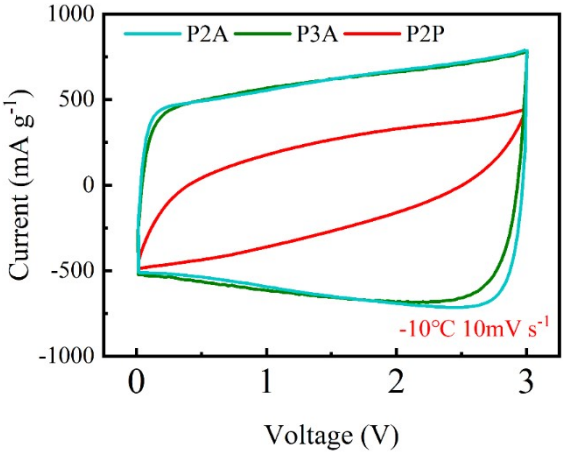

Fig.S12 CV curves of the SCs with three ILQSEs at -10℃

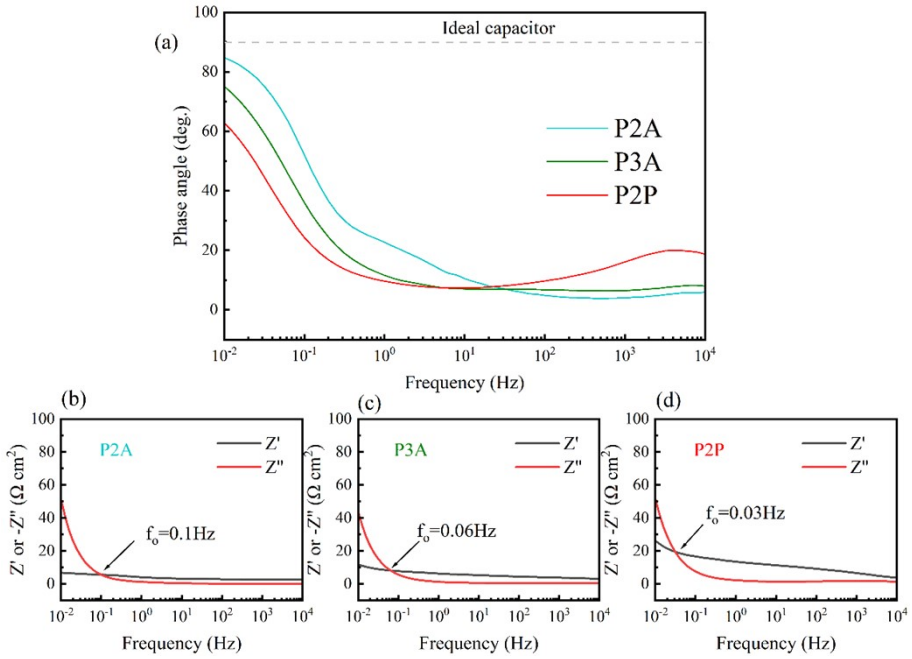

Fig.S13 (a) Phase angle as a function of frequency in the SCs with three ILQSEs; (b) Bode plots (Z' or Z'' as a function of frequency) of the SCs with (b) P2A, (c) P3A and (d) P2P, respectively

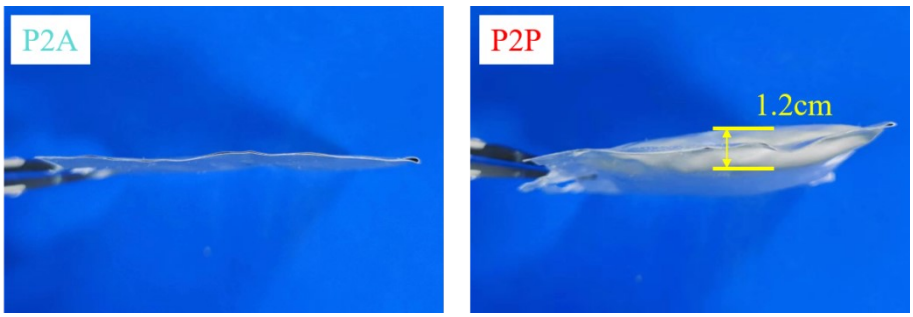

Fig.S14 Cross-section pictures of the flexible SCs after 10000 cycles

Supplementary Tables

Table S1 Several parameters obtained from the EIS measurements of the SCs

Sample	R_b /Ω	R_{ct} /Ω	σ_0 /Ω	D /cm^2 s^{-1}	i_0 /mA cm^{-2}	τ /s	f_o /Hz	τ_0 /s
P2A	2.318	0.386	3.482	1.526	0.043	0.011	0.1	10
P3A	2.488	1.057	4.884	0.776	0.016	0.022	0.06	16.67
P2P	2.497	8.834	5.012	0.319	0.002	0.053	0.03	33.34

Additional References

[1] J. Li, T. Zhang, X. Hui, R. Zhu, Q. Sun, X. Li, L. Yin, Competitive Li+ Coordination in Ionogel Electrolytes for Enhanced Li-Ion Transport Kinetics, *Adv. Sci.*, 2023**,** 2300226.

[2] H. He, Y. Wang, M. Li, J. Qiu, Y. Wen, J. Chen, In situ cross-linked fluorinated gel polymer electrolyte based on PEGDA-enabled lithium-ion batteries with a wide temperature operating range, *Chem. Eng. J.*, 2023**, 467**, 143311.

[3] H. Ji, X. Zhao, Z. Qiao, J. Jung, Y. Zhu, Y. Lu, L.L. Zhang, A.H. MacDonald, R.S. Ruoff, Capacitance of carbon-based electrical double-layer capacitors, *Nat. Commun.*, 2014**, 5**, 3317.

[4] S.-Y. Lu, M. Jin, Y. Zhang, Y. B. Niu, J. C. Gao, C.M. Li, Chemically Exfoliating Biomass into a Graphene-like Porous Active Carbon with Rational Pore Structure, Good Conductivity, and Large Surface Area for High-Performance Supercapacitors, *Adv. Energy Mater.*, 2018**, 8**, 1702545.

[5] Y. Song, T. Liu, M. Li, B. Yao, T. Kou, D. Feng, F. Wang, Y. Tong, X.X. Liu, Y. Li, Engineering of Mesoscale Pores in Balancing Mass Loading and Rate Capability of Hematite Films for Electrochemical Capacitors, *Adv. Energy Mater.*, 2018**, 8**, 1801784.

[6] Y. Li, Q. Gong, X. Liu, Z. Xia, Y. Yang, C. Chen, C. Qian, Wide temperature-tolerant polyaniline/cellulose/polyacrylamide hydrogels for high-performance supercapacitors and motion sensors, *Carbohydr. Polym.*, 2021**, 267**, 118207.

[7] S. Peng, X. Jiang, X. Xiang, K. Chen, G. Chen, X. Jiang, L. Hou, High-performance and flexible solid-state supercapacitors based on high toughness and thermoplastic poly(vinyl alcohol)/NaCl/glycerol supramolecular gel polymer electrolyte, *Electrochim. Acta*, 2019**, 324**, 134874.

[8] B. Dharmasiri, F. Stojcevski, K.A.S. Usman, S. Alex Qin, J.M. Razal, E.H. Doeven, P.S. Francis, T.U. Connell, Y. Yin, G.G. Andersson, A. Borkar, L.C. Henderson, Flexible carbon fiber based structural supercapacitor composites with solvate ionic liquid-epoxy solid electrolyte, *Chem. Eng. J.*, 2023**, 455**, 140778.

[9] F. Wang, H. Liu, Y. Guo, Q. Han, P. Lou, L. Li, J. Jiang, S. Cheng, Y. Cao, In Situ High‐performance Gel Polymer Electrolyte with Dual‐reactive Cross‐linking for Lithium Metal Batteries, *Energy Environ. Mater.*, 2023**, 0**, e12497.